PERGAMON

Building and Environment 37 (2002) 705–712

BUILDING AND ENVIRONMENT

www.elsevier.com/locate/buildenv

A numerical investigation of effects of a moving operator on airflow patterns in a cleanroom

Suh-Jenq Yang[a], Wu-Shung Fu[b,*]

[a] Department of Industrial Engineering and Management, Nan Kai College, Tsaotun, Nantou, 54210, Taiwan
[b] Department of Mechanical Engineering, National Chiao Tung University, Hsinchu 30056, Taiwan, ROC

Received 25 May 2000; received in revised form 21 June 2000; accepted 31 July 2001

Abstract

The variations of the airflow induced by a moving operator in a cleanroom installed with a curtain were studied numerically. This situation is cataloged to a class of the moving boundary problems. An arbitrary Lagrangian–Eulerian kinematic description method is utilized to describe the flow field and a penalty finite element formulation with moving meshes is adopted to solve this problem. The effects of the moving operator and curtain on the airflow patterns under different distances from the workbench to the curtain with the moving speed of the operator equal to 2.0 and Reynolds number $Re = 500$ are taken into account. The results show that recirculation zones are formed around the operator and workbench due to the movement of the operator. The recirculation zones are not favorable to the cleanroom because they may induce a local turbulent flow and entrain and trap contaminants. These phenomena are remarkably different from those of the moving operator assumed as stationary in the cleanroom. Based on the length of the curtain, it is useful for protecting the operator from the hazardous gases.

Keywords: Cleanroom; Curtain; Moving operator; ALE; Recirculation zones

1. Introduction

Cleanroom recently became an indispensable environment in the pharmaceutical, medical technology, and semiconductor industries for producing high quality and precision products. Since the external air entering the cleanroom must be filtered by the HEPA or ULPA filter banks, the operators and equipment become the major sources of the contaminants in the cleanroom [1]. Most particles generated by the above sources are continuously swept away by the airflow from the ceiling of the cleanroom. Some residual particles, which may be suspended within recirculation zones or deposited on the products and equipment by gravitational settling, diffusion, collision, and electrostatic attraction, etc., are extremely difficult to be removed by the airflow. How to remove these residual particles effectively becomes an important issue in the semiconductor industry.

Concerning the motions of the airflow and particles in the cleanroom, several studies investigated this subject. Ermak and Buckholz [2] adopted a Monte Carlo method to simulate the effects of the airflow on the particles, and the results showed that the characteristics of the particle transport were dominated by the airflow. Kuehn [3], Yamamoto et al. [4], Busnaina et al. [5], and Lemaire and Luscure [6] utilized the numerical modeling to study the airflow and particle transport in the cleanroom. Liu and Ahn [7] used the analogy between mass transfer and heat transfer to determine particle deposition rates by diffusion. Settles and Via [8] adopted Schloeren observation to observe the flow paths of the particles in the cleanroom. Furthermore, Marvell [9] summarized the factors of effect on the airflow and contaminant transport in a minienvironment system. Tannous [10] utilized the computational fluid dynamics method to investigate the flow field of a minienvironment in the cleanroom.

However, for facilitating the analysis, most previous studies regarded a moving operator as a stationary object, which resulted in the phenomena of the airflow in the cleanroom being rather different from the realistic situation. Besides, a curtain is usually employed in the cleanroom to divide the inlet of the airflow into two sections and protect the operator from hazardous gases while processing. One section uses well-filtered air at a higher flow rate to sweep away the particles suspended near the working area and the other uses air filtered at a lower flow rate for saving energy. To the knowledge of the authors, the effects of both

* Corresponding author. Tel.: +886-3-5712121; fax: 886-3-5720634.
E-mail address: wsfu@cc.nctu.edu.tw (W.-S. Fu).

0360-1323/02/$ - see front matter
PII: S0360-1323(01)00080-4

Notation

h_0	dimensional height of the operator [m]
H_0	dimensionless height of the operator
h_1	dimensional height of the cleanroom [m]
H_1	dimensionless height of the cleanroom
h_2	dimensional distance from the outlet of the cleanroom to the operator [m]
H_2	dimensionless distance from the outlet of the cleanroom to the operator
h_3	dimensional distance from the workbench to the curtain [m]
H_3	dimensionless distance from the workbench to the curtain
h_4	dimensional height of the workbench [m]
H_4	dimensionless height of the workbench
p	dimensional pressure [N/m^2]
p_∞	reference pressure [N/m^2]
P	dimensionless pressure
Re	Reynolds number
t	dimensional time [s]
u, v	dimensional velocities of the airflow in x- and y-direction [m/s]
U, V	dimensionless velocities of the airflow in X- and Y-direction
u_b	dimensional moving velocity of the operator [m/s]
U_b	dimensionless moving velocity of the operator
$\hat{u}$	dimensional mesh velocity in x-direction [m/s]
$\hat{U}$	dimensionless mesh velocity in X-direction
v_0	dimensional airflow inlet velocity at section $\overline{CD}$ [m/s]
V_0	dimensionless airflow inlet velocity at section $\overline{CD}$
v_1	dimensional airflow inlet velocity at section $\overline{AB}$ [m/s]
V_1	dimensionless airflow inlet velocity at section $\overline{AB}$
w	dimensional width of the cleanroom [m]
W	dimensionless width of the cleanroom
w_0	dimensional width of the operator [m]
W_0	dimensionless width of the operator
w_1	dimensional width of the airflow inlet at section $\overline{AB}$ [m]
W_1	dimensionless width of the airflow inlet at section $\overline{AB}$
w_2	dimensional width of the curtain [m]
W_2	dimensionless width of the curtain
w_3	dimensional width of the airflow inlet at section $\overline{CD}$ [m]
W_3	dimensionless width of the airflow inlet at section $\overline{CD}$
w_4	dimensional width of the workbench [m]
W_4	dimensionless width of the workbench
w_5	dimensional distance from the workbench to the operator [m]
W_5	dimensionless distance from the workbench to the operator
x, y	dimensional Cartesian coordinates [m]
X, Y	dimensionless Cartesian coordinates

Greek symbols

λ	penalty parameter
ν	kinematic viscosity [m^2/s]
ρ	density [kg/m^3]
τ	dimensionless time
Ψ	dimensionless stream function

Superscripts

(e)	element
m	iteration number
T	transpose matrix

Other

[ ]	matrix
{ }	column vector
⟨ ⟩	row vector

the moving operator and curtain on the airflow are hardly investigated, and minimum literature is available on this subject.

Consequently, the aim of this paper is to investigate the variations of the airflow patterns induced by the movement of the operator in the cleanroom numerically. In addition, three different lengths of the curtain are taken into consideration to examine the effects of the length of the curtain on the airflow patterns. Due to the movement of the operator, this problem is classified into a class of the moving boundary problems, and is hardly analyzed by either the Lagrangian or Eulerian kinematic description method solely. An arbitrary Lagrangian–Eulerian (ALE) kinematic description method [11–13], which combines the characteristics of the Lagrangian and Eulerian methods, is an appropriate method to describe this problem. In the ALE method, the computational meshes may move with the fluid (Lagrangian), be held fixed (Eulerian), or be moved in any other prescribed way. The details of the ALE method are delineated by Hirt et al. [11], Hughus et al. [12], and Ramaswamy

[13]. A Galerkin finite element method with moving meshes and a backward difference scheme, dealing with the time terms, are used to solve the governing equations. The results show that the length of the curtain and the movement of the operator significantly influence the airflow patterns in the cleanroom. These phenomena are quite different from those regarded the moving operator as a stationary one.

2. Physical model

A two-dimensional vertical laminar flow cleanroom as sketched in Fig. 1 is used. The width and height of the cleanroom are $w(=w_1+w_2+w_3)$ and h_1, respectively. A rectangular block with height h_0 and width w_0 is used to simulate an operator in the cleanroom. The distance from the outlet of the cleanroom to the bottom surface of the operator is h_2. A workbench with height h_4 and width $w_4(=w_1+w_2)$ is set on the left side of the cleanroom. A curtain with width w_2 is mounted on the inlet ceiling and divides the inlet airflow into two sections, $\overline{AB}$ and $\overline{CD}$. The distance from the workbench to the curtain is h_3. Two different inlet air velocities are v_1 and v_0 flowing separately at the inlet sections $\overline{AB}$ and $\overline{CD}$. Initially ($t=0$), the operator is stationary and the airflow is flowing steadily, and the distance from the workbench to the operator is w_5. As the time $t>0$, the operator moves to the workbench with a constant velocity u_b and remains beside the workbench. Finally, the operator leaves the workbench and moves back to the original place. The interaction between the inlet airflow and moving operator affects the behavior of the airflow patterns and contaminant diffusion in the cleanroom. This problem becomes time-dependent and can be cataloged to a class of moving boundary problems. As a result, the ALE method is properly utilized to analyze this problem.

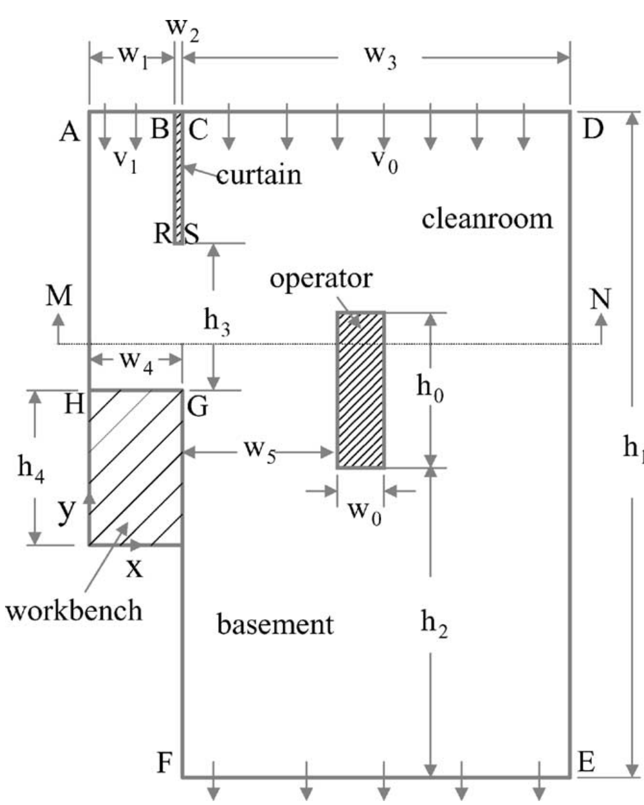

Fig. 1. Physical model.

In order to facilitate the analysis, the following assumptions are made.

(1) The fluid is air and the flow field is two-dimensional, incompressible and laminar.
(2) The fluid properties are constant and the effect of the gravity is neglected.
(3) The no-slip condition is held at the interface between the fluid and operator.

Based upon the characteristic scales of w_0, v_0 and ρv_0^2, the dimensionless variables are defined as follows:

$$X=\frac{x}{w_0},\quad Y=\frac{y}{w_0},\quad U=\frac{u}{v_0},$$

$$V=\frac{v}{v_0},\quad \hat{U}=\frac{\hat{u}}{v_0},\quad U_b=\frac{u_b}{v_0},$$

$$P=\frac{p-p_\infty}{\rho v_0^2},\quad \tau=\frac{tv_0}{w_0},\quad Re=\frac{v_0 w_0}{\nu},\tag{1}$$

where $\hat{u}$ is the mesh velocity and u_b is the moving velocity of the operator.

According to the above assumptions and dimensionless variables, the dimensionless ALE governing equations are expressed as the following equations:

Continuity equation

$$\frac{\partial U}{\partial X}+\frac{\partial V}{\partial Y}=0,\tag{2}$$

Momentum equations

$$\frac{\partial U}{\partial \tau}+(U-\hat{U})\frac{\partial U}{\partial X}+V\frac{\partial U}{\partial Y}=-\frac{\partial P}{\partial X}+\frac{1}{Re}\left(\frac{\partial^2 U}{\partial X^2}+\frac{\partial^2 U}{\partial Y^2}\right),\tag{3}$$

$$\frac{\partial V}{\partial \tau}+(U-\hat{U})\frac{\partial V}{\partial X}+V\frac{\partial V}{\partial Y}=-\frac{\partial P}{\partial Y}+\frac{1}{Re}\left(\frac{\partial^2 V}{\partial X^2}+\frac{\partial^2 V}{\partial Y^2}\right).\tag{4}$$

As the time $\tau>0$, the boundary conditions are as follows:

On the wall surfaces $\overline{DE}$, $\overline{FG}$, $\overline{GH}$, and $\overline{AH}$

$$U=V=0.\tag{5}$$

On the curtain surfaces $\overline{BR}$, $\overline{CS}$, and $\overline{RS}$,

$$U=V=0.\tag{6}$$

On the airflow inlet section $\overline{\mathrm{AB}}$

$$U=0, \quad V=-1.25. \tag{7}$$

On the airflow inlet section $\overline{\mathrm{CD}}$

$$U=0, \quad V=-1.0. \tag{8}$$

On the airflow outlet section $\overline{\mathrm{EF}}$

$$\partial U/\partial Y=\partial V/\partial Y=0. \tag{9}$$

On the interface of the operator and the airflow

$$U=U_{\mathrm{b}}, \quad V=0. \tag{10}$$

3. Numerical method

A Galerkin finite element method with moving meshes and a backward scheme to deal with the time terms are adopted to solve the governing equations (2)–(4). A penalty function [14] and the Newton–Raphson iteration algorithm are utilized to simplify the pressure and nonlinear terms in the momentum equations, respectively. The velocity terms are approximated by quadrilateral and nine-node quadratic isoparametric elements. The discretization processes of the governing equations are similar to those used by Fu et al. [15] and Huebner et al. [16]. Then, the momentum equations (3) and (4) can be expressed as follows:

$$\sum_{l}^{n_e}([A]^{(\mathrm{e})}+[K]^{(\mathrm{e})}+\lambda[L]^{(\mathrm{e})})\{q\}_{\tau+\Delta\tau}^{(\mathrm{e})}=\sum_{l}^{n_e}\{f\}^{(\mathrm{e})}, \tag{11}$$

where

$$(\{q\}_{\tau+\Delta\tau}^{(\mathrm{e})})^{\mathrm{T}}=\langle U_1,U_2,\ldots,U_9,V_1,V_2,\ldots,V_9\rangle_{\tau+\Delta\tau}^{m+1}, \tag{12}$$

$[A]^{(\mathrm{e})}$ includes the (m)th iteration values of U and V at time $\tau+\Delta\tau$,

$[K]^{(\mathrm{e})}$ includes the shape function, $\hat{U}$ and time differential terms,

$[L]^{(\mathrm{e})}$ includes the penalty function terms,

$\{f\}^{(\mathrm{e})}$ includes the known values of U and V at time τ and (m)th iteration values of U and V at time $\tau+\Delta\tau$.

In Eq. (11), the terms with the penalty parameter, λ, are integrated by 2×2 Gaussian quadrature, and the other terms are integrated by 3×3 Gaussian quadrature. The value of penalty parameter used in this study is 10^6 and the frontal method solver [17,18] is utilized to solve Eq. (11).

Concerning the mesh velocity $\hat{U}$, it is linearly distributed and inversely proportional to the distance between the nodes of the computational meshes and the operator in this study. The mesh velocity near the operator is faster than that near the boundaries of the computational domain. In addition, the boundary layer thickness on the operator surface is extremely thin and can be approximately estimated by $Re^{-1/2}$ [19]. To avoid the computational nodes in the vicinity of the operator slipping away from the boundary layer, the mesh velocities adjacent to the operator are expediently assigned equal to the velocity of the operator.

A brief outline of the solution procedures are described as follows:

(1) Determine the optimal mesh distribution and number of the elements and nodes.
(2) Solve the values of U and V at the steady state and regard them as the initial values.
(3) Determine the time increment $\Delta\tau$ and the mesh velocities $\hat{U}$ at every node.
(4) Update the coordinates of the nodes and examine the determinant of the Jacobian transformation matrix to ensure the one-to-one mapping to be satisfied during the Gaussian quadrature numerical integration, otherwise, execute the mesh reconstruction.
(5) Solve Eq. (11), until the following criteria for convergence are satisfied:

$$\left|\frac{\phi^{m+1}-\phi^{m}}{\phi^{m+1}}\right|_{\tau+\Delta\tau}<10^{-3}, \quad \text{where } \phi=U,V \tag{13}$$

(6) Continue the next time step calculation until the assigned position of the operator is reached.

4. Results and discussion

The length of the curtain plays an important role for protecting the wafer on the workbench, than three different dimensionless distances from the workbench to the curtain, $H_3=6.0$, 3.0, and 2.0, which correspond to cases 1, 2 and 3, respectively, is listed in Table 1. At time $\tau=0.0$, the distance from the operator to the workbench is $W_5=4.5$. For satisfying the velocity boundary conditions at the inlet and outlet, the dimensionless lengths of $H_1(=h_1/w_0)$ and $H_2(=h_2/w_0)$ are determined by numerical tests.

Generally, the walking speed of the operator is twice the inlet speed of the airflow in the cleanroom. The phenomena of the moving speed of the operator being equal to 2.0 (the moving velocity of the operator, U_{b}, may be 2.0 or -2.0) and $Re=500$ are analyzed in detail. For obtaining an optimal computational mesh, three different nonuniform distribution elements 3612, 4048, and 4804 (corresponding to 14816, 16572, and 19640 nodes, respectively) are tested for case 2 at the steady state. The results of the velocities U and

Table 1
The dimensionless geometric lengths of the cleanroom for three different cases

	W_0	W_1	W_2	W_3	W_4	H_0	H_1	H_2	H_3	H_4
case 1	1.0	2.3	0.2	12.5	2.5	6.0	30.0	18.0	6.0	6.0
case 2	1.0	2.3	0.2	12.5	2.5	6.0	34.0	18.0	3.0	6.0
case 3	1.0	2.3	0.2	12.5	2.5	6.0	30.0	18.0	2.0	6.0

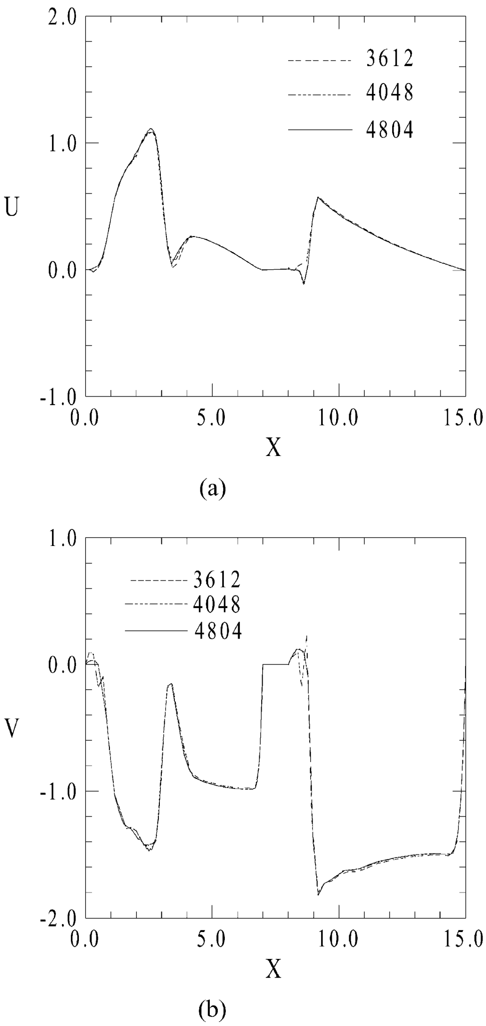

Fig. 2. Comparison of the distributions of the velocities U and V along the line $\overline{MN}$ for case 2 at steady state under different meshes. (a) X-U, and (b) X-V.

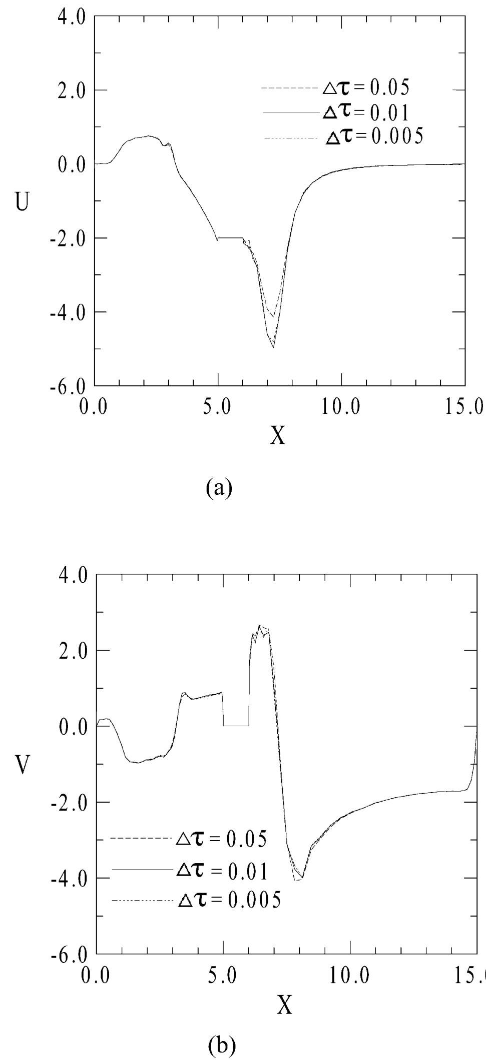

Fig. 3. Comparison of the distribution of the velocities U and V along the line $\overline{MN}$ at time $\tau = 2.0$ for case 2 at $U_b = -2.0$ under different time steps (a) X-U, and (b) X-V.

V distributions along the line $\overline{MN}$ as indicated in Fig. 1 are shown in Fig. 2. Based upon the results, the computational mesh with 4804 elements is adopted for case 2. Similarly, the computational meshes with 4644 and 4560 elements (corresponding to 18964 and 18664 nodes, respectively) are adopted for cases 1 and 3, respectively.

As for the selection of the time step $\Delta\tau$, three different time steps 0.05, 0.01 and 0.005 at $U_b = -2.0$ are tested for case 2. The distributions of the velocities U and V along the line $\overline{MN}$ at time $\tau = 2.0$ are shown in Fig. 3. The result of the velocities U and V for different time steps is quite consistent. The time step $\Delta\tau = 0.01$ is chosen for all cases.

The dimensionless stream function Ψ is defined as

$$U = \frac{\partial \Psi}{\partial Y} \quad \text{and} \quad V = -\frac{\partial \Psi}{\partial X}. \tag{14}$$

For illustrating the flow field clearly, the phenomena of the streamlines around the work region of the cleanroom are presented exclusively. However, it should be noted that the computational domain included a much larger region than what is displayed in the subsequent figures.

The transient developments of the streamline distributions for case 1 ($H_3 = 6.0$) are shown in Fig. 4. In this case, the height of the top surface of the operator is lower than the bottom surface of the curtain. At time $\tau = 0.0$, as shown in Fig. 4(a), the operator is stationary and the airflow is flowing steadily. Recirculation zones are found near the top and lateral surfaces of the workbench. As time $\tau > 0.0$, the operator starts to move towards the workbench with a constant velocity $U_b = -2.0$, and the variations of the flow field attain a transient state. As shown in Fig. 4(b), the space between the workbench and operator is contracted gradually, which results in the inlet airflow beginning to flow over the rear region of the operator. Since the operator moves toward the workbench, the operator pushes the airflow before the operator, and the direction of this airflow is forced to be

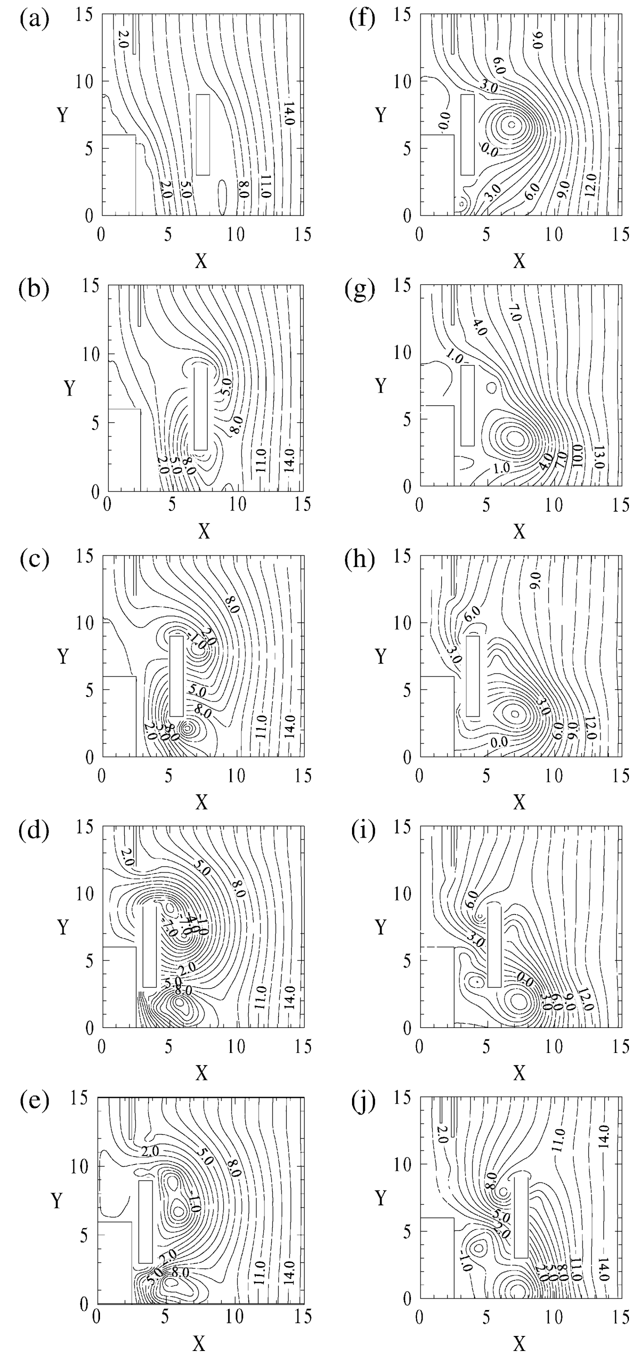

Fig. 4. The transient developments of the streamline distributions around the work region of the cleanroom for case 1 (a) $\tau = 0.0$, $U_b = 0.0$, (b) $\tau = 0.2$, $U_b = -2.0$, (c) $\tau = 1.0$, $U_b = -2.0$, (d) $\tau = 2.0$, $U_b = -2.0$, (e) $\tau = 2.2$, $U_b = 0.0$, (f) $\tau = 4.5$, $U_b = 0.0$, (g) $\tau = 7.0$, $U_b = 0.0$, (h) $\tau = 7.2$, $U_b = 2.0$, (i) $\tau = 8.0$, $U_b = 2.0$, and (j) $\tau = 9.0$, $U_b = 2.0$.

changed and to flow toward the workbench remarkably. In the meantime, the airflow in the vicinity of the rear region of the operator and the top and bottom surfaces of the operator simultaneously replenishes the vacant space induced by the movement of the operator. As a result, new recirculation zones are formed around the operator. As the time increases, the space between the workbench and operator becomes narrower, then most inlet airflow flows through the rear region of the operator, as shown in Figs. 4(c)–(d). In this duration, the airflow induced by the movement of the operator is forced to flow over the top surface of the operator, which causes the recirculation zones in the rear region of the operator to enlarge gradually. From a viewpoint of fluid mechanics, these recirculation zones are not favorable to the cleanroom because they may induce a local turbulent flow near the operator and workbench and entrain and trap particles. Particles may escape from these recirculation zones due to the effects of the inertia force, gravitational settling, turbulent diffusion, Brownian diffusion, electrostatic force, or other forces and deposit on the workbench to pollute the products. These phenomena are very complex and can hardly be predicted by both the experimental and numerical methods.

For the duration of time τ from 2.0 to 7.0, the operator stays beside the workbench ($U_b = 0.0$), as indicated in Figs. 4(e)–(g). Since the space between the workbench and operator is narrow, the airflow passing through this space is slight and most of the airflow from the inlet flow through the rear region of the operator. As a result, the recirculation zones around the operator migrate to the downstream and shrink gradually by the airflow from the inlet. But large recirculation zones are observed around the top surface of the workbench. This flow may cause the particles to deposit on the product.

As time $\tau > 7.0$, as shown in Figs. 4(h)–(j), the operator begins to leave the workbench with a constant velocity $U_b = 2.0$. Because of the operator moving toward the right, the airflow from the inlet is affected by the movement of the operator and also flows toward the right, which causes the recirculation zones near the workbench and operator to be destroyed gradually. Furthermore, the space mentioned above becomes broad gradually, and the inlet airflow easily passes through this space and replenishes the vacant space induced by the movement of the operator. Thus, new recirculation zones appear near the top and bottom surfaces of the operator and extend to the lower region beside the workbench.

Fig. 5 shows the transient developments of the streamline distributions for case 2 ($H_3 = 3.0$) in which the height of the top surface of the operator is equal to the bottom surface of the curtain. At the beginning of the transient state, the operator moves toward the workbench with a constant velocity $U_b = -2.0$ and these phenomena are similar to case 1. As the time increases, the space between the workbench and operator is contracted gradually, and some airflows from the inlet section $\overline{AB}$ circumvent the curtain and flow over the rear region of the operator (Fig. 5(c)). As a result, the curtain protects the operator from the hazardous gases. Later, the airflow flowing around the curtain interacts with the airflow from the section $\overline{CD}$, and large recirculation zones appear around the operator while small new recirculation zones are observed around the curtain, as shown in

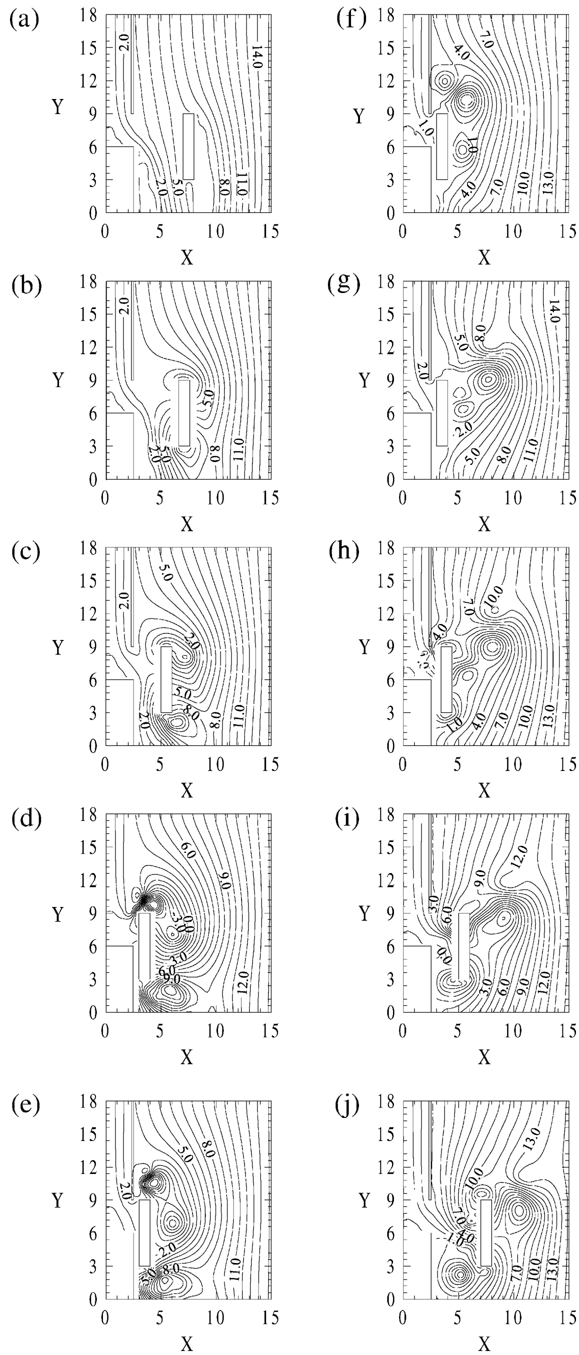

Fig. 5. The transient developments of the streamline distributions around the work region of the cleanroom for case 2 (a) $\tau = 0.0$, $U_b = 0.0$, (b) $\tau = 0.2$, $U_b = -2.0$, (c) $\tau = 1.0$, $U_b = -2.0$, (d) $\tau = 2.0$, $U_b = -2.0$, (e) $\tau = 2.2$, $U_b = 0.0$, (f) $\tau = 4.5$, $U_b = 0.0$, (g) $\tau = 7.0$, $U_b = 0.0$, (h) $\tau = 7.2$, $U_b = 2.0$, (i) $\tau = 8.0$, $U_b = 2.0$, and (j) $\tau = 9.0$, $U_b = 2.0$.

Fig. 5(d). Besides, due to the existence of the curtain, small recirculation zones around the top surface of the workbench cannot be destroyed by the airflow, which is different from that of case 1 as shown in Fig. 4(d).

During time τ from 2.0 to 7.0, as shown in Figs. 5(e)–(g), the operator remains beside the workbench ($U_b = 0.0$). Some airflows from the inlet section $\overline{AB}$ flow through the space between the curtain and operator, and then flow over the rear region of the operator. Thus, the recirculation zones around the curtain enlarge gradually and extend farther, as shown in Figs. 5(e)–(f). As the time increases, these recirculation zones are destroyed by the airflow circumventing the curtain and the airflow from the inlet section $\overline{CD}$, as indicated in Fig. 5(g). Furthermore, due to the existence of the curtain, the recirculation zones near the top surface of the workbench are shrunk gradually, which is beneficial to the contamination control.

As time $\tau > 7.0$, as shown in Figs. 5(h)–(j), the operator leaves the workbench with a constant velocity $U_b = 2.0$. In this situation, the variations of the flow fields are similar to case 1 as shown in Figs. 4(h)–(j).

Fig. 6 shows the transient developments of the streamline distributions for case 3 ($H_3 = 2.0$) in which the height of the top surface of the operator is higher than the bottom surface of the curtain. The variations of the airflow patterns for this case are more slightly drastic than that of case 2. As the operator moves toward the workbench, the space between the curtain and operator is contracted gradually. As Figs. 6(b)–(d) show, due to the obstruction of the curtain, the airflow from the inlet section $\overline{AB}$ circumventing the curtain is difficult and mass flow rate of the airflow through the space between the curtain and operator is smaller than that of case 2. Consequently, the recirculation zones around the top surface of the workbench is shrunk. Besides, the operator seems to be an obstruction in the way of the airflow passing through the space between the curtain and workbench, then the variations of the recirculation zones behind the operator become more apparent than the former ones.

5. Conclusions

The effects of a moving operator and curtain on the variations of the airflow patterns in a vertical laminar cleanroom are investigated numerically. The results can be summarized as follows:

1. The moving operator affects the variations of the airflow patterns in the cleanroom very much. Recirculation zones are observed around the operator and workbench as the operator approaches the workbench. These phenomena are remarkably different from those of the moving operator regarded as a stationary object in the cleanroom of the previous studies.
2. The curtain can usually protect the operator from the hazardous gases as the distance between the workbench and curtain is small.
3. The curtain may confine the flowing of the airflow from the inlet and force the recirculation zones around the top surface of the workbench shrunk gradually when the operator remained beside the workbench.

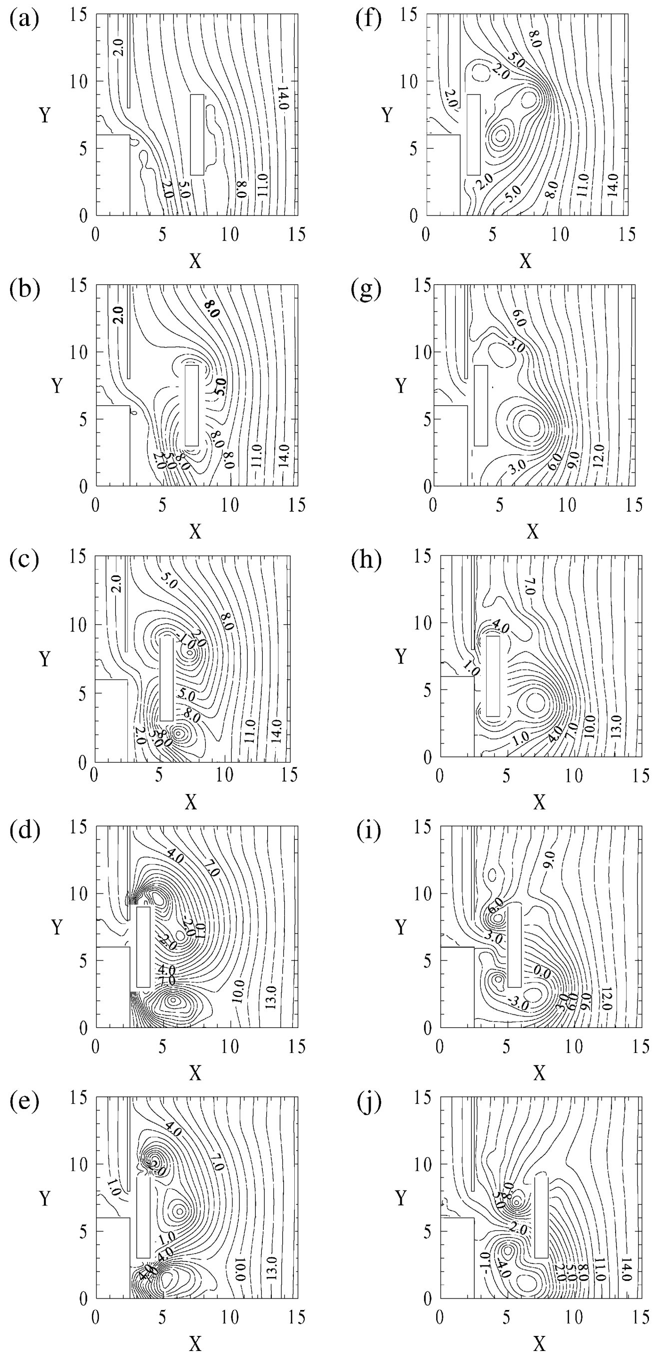

Fig. 6. The transient developments of the streamline distributions around the work region of the cleanroom for case 3 (a) $\tau = 0.0$, $U_b = 0.0$, (b) $\tau = 0.2$, $U_b = -2.0$, (c) $\tau = 1.0$, $U_b = -2.0$, (d) $\tau = 2.0$, $U_b = -2.0$, (e) $\tau = 2.2$, $U_b = 0.0$, (f) $\tau = 4.5$, $U_b = 0.0$, (g) $\tau = 7.0$, $U_b = 0.0$, (h) $\tau = 7.2$, $U_b = 2.0$, (i) $\tau = 8.0$, $U_b = 2.0$, and (j) $\tau = 9.0$, $U_b = 2.0$.

Acknowledgements

The support of this work by the National Science Council of Taiwan, R.O.C., under contract NSC90-2626-E-252-003 is gratefully acknowledged.

References

[1] Gilmore JS. Ultrafine particles. In: Donovan RP, editor. Particle control for semiconductor manufacturing. New York: Marcel Dekker Inc., 1990. p. 79–103.
[2] Ermak DL, Buckholz H. Numerical integration of the Langerin equation: Monte Carlo simulation. Journal of Computational Physics 1980;35:169–82.
[3] Kuehn TH. Computer simulation of airflow and particle transport in cleanrooms. Journal of Environmental Science 1988;31(5):21–7.
[4] Yamamoto T, Donovan RP, Ensor DS. Model study for optimization of cleanroom airflow. Journal of Environmental Science 1988;31(6):24–9.
[5] Busnaina AA, Abuzeid S, Sharif MAR. Numerical modeling of fluid flow and particle transport in clean room. Proceedings of the Ninth International Committee Contamination Control Societies Conference, Los Angeles, 1988. p. 600–7.
[6] Lemaire T, Luscuere P. Investigating computer modeling of cleanroom airflow patterns. Microcontamination 1991;9(8):19–26.
[7] Liu BYH, Anh K. Particle deposition on semiconductor wafers. Aerosol Science and Technology 1987;6(3):215–24.
[8] Settles GS, Via GG. A portable Schlieren system for clean-room airflow analysis. Journal of Environmental Science 1988;30(5):17–21.
[9] Marvell G. Minienvironment air flow dynamics. Solid State Technology 1993;36(8):47–8.
[10] Tannous AG. Air flow simulation in a minienvironment. Solid State Technology 1996;39(7):201–9.
[11] Hirt CW, Amsden AA, Cooks HK. An arbitrary Lagrangian–Eulerian computing method for all flow speeds. Journal of Computational Physics 1974;14:227–53.
[12] Hughes TJR, Liu WK, Zimmermann TK. Lagrangian–Eulerian finite element formulation for incompressible viscous flows. Computer Methods in Applied Mechanics and Engineering 1981;29:329–49.
[13] Ramaswamy B. Numerical simulation of unsteady viscous free surface flow. Journal of Computational Physics 1990;90:396–430.
[14] Reddy JN, Gartling DK. The finite element method in heat transfer and fluid dynamics. Ann. Arbor: CRC Press. Inc., 1994. p. 145–51.
[15] Fu WS, Kau TM, Shieh WJ. Transient laminar natural convection in an enclosure from steady flow state to stationary state. Numerical Heat Transfer A 1990;18:189–211.
[16] Hueber KH, Thornton EA, Byrom TG. The finite element method for engineers. 3rd ed. New York: Wiley, 1995. p. 406–15.
[17] Irons BM. A frontal solution program for finite element analysis. International Journal for Numerical Methods in Engineering 1970;2:5–32.
[18] Taylor C, Hughes TG. Finite element programming of the Navier–Stokes Equations. UK: Pineridge Press Ltd., 1981 [Chapter 6].
[19] Schlichting H. Boundary layer theory, 7th ed. New York: McGraw-Hill, 1979 [Chapter 5].